RSC Advances

ROYAL SOCIETY OF CHEMISTRY

www.rsc.org/advances

Rod-like $NaNbO_3$: mechanisms for stable solvothermal synthesis, temperature-mediated phase transitions and morphological evolutions

Qilin Gu, [1, 2] Kongjun Zhu, [1*] Jinsong Liu, [2] Pengcheng Liu, [1, 2] Yang Cao, [3] Jinhao Qiu[1]

[1]State Key Laboratory of Mechanics and Control of Mechanical Structures, College of Aerospace Engineering, Nanjing University of Aeronautics and Astronautics, Nanjing, 210016, P. R. China

[2]College of Materials Science and Engineering, Nanjing University of Aeronautics and Astronautics, Nanjing 210016, China

[3]Center for Interdisciplinary Research, Tohoku University, Sendai, Miyagi 982, Japan

***Corresponding Author:** E-mail address: kjzhu@nuaa.edu.cn

Abstract

One dimensional (1D) $NaNbO_3$ powders have attracted increasing attentions for their excellent photo-catalytic and piezoelectric properties, and the stable, moderate and low-energy synthesis of the targets is highly desirable. Herein, a facial solvothermal strategy is adapted to synthesize the one-dimensional (1D) rod-like precursors $Na_7(H_3O)Nb_6O_{19}\cdot 14H_2O$ by using isopropanol as reaction medium. When the precursor is subjected to post-heating treatments, rod-like orthorhombic as well as approximate ellipsoids-like monoclinic $NaNbO_3$ powders are obtained. Corresponding mechanisms for the stable solvothermal synthesis, morphological evolution and phase transition are further proposed and discussed.

1. Introduction

Sodium niobates ($NaNbO_3$), which are indispensable members of the alkaline niobates, have emerged as vital functional materials with many technological and scientific applications, [1, 2] such as energy recovery, intelligent sensors, health monitoring, acoustic transducers, dielectric waveguides, holographic data storage, and piezoelectric actuators, because of their excellent nonlinear optical,[3] ferroelectric,[4] piezoelectric,[5, 6] pyro-electric,[7] and photo-catalytic[8] properties as well as their environmental friendly advantages.

$NaNbO_3$ has rich phase structures, such as orthorhombic, tetragonal, and cubic, among others.[9-11] As such, explorations of the applications of some unusual phases, *e.g.*, rhombohedral and monoclinic, are of great significance.[12, 13] Among the past decades, $NaNbO_3$ with diversiform morphologies, including cubes, rods, wires, dandelions, and octahedrons, have be synthesized through various synthetic strategies and processing parameters.[14] Thanks to their orientation and high aspect ratio value, one-dimensional (1D) nanowires/rods of $NaNbO_3$ have outstanding properties both in photo-catalysts[15] and piezoelectric nano-generators.[16] To the best of our knowledge, rod-like $NaNbO_3$ has been obtained through molten-salt reaction *via* ion-exchange using $K_2Nb_8O_{21}$ nanowires as ~~a~~ starting templates.[17] Furthermore, $NaNbO_3$ nanowires can be achieved by annealing the hydrothermally synthesized $Na_2Nb_2O_6$ nanowires.[18–24] However, both synthesis strategies have intrinsic disadvantages. The molten-salt reaction is unsuitable for large-scale synthesis given its high energy consumption and safety hazards, while the mass production of $NaNbO_3$ nanowires is

infeasible because the formation of $Na_2Nb_2O_6$ nanowire requires highly alkaline conditions (10–15 M) and is sensitive to process parameters, such as the reaction temperature and time. Up to now, the controllable, moderate and low-energy synthesis of 1D $NaNbO_3$ powders is still a meaningful project with challenges.

Previous studies[25-29] indicated that addition of IPA can effectively reduce the required alkaline concentration of the niobate reaction system. Water is also reported to be unsuitable for the synthesis of many inorganic metal oxides in crystalline states.[30] Moreover, solvothermal has been proved to be an advantaged approach to synthesize kinds of inorganic materials, [31, 32] since organic solvents with better transport properties can accelerate chemical reactions, especially when reaction temperature is approximate to or above its critical point. [33, 34] Limited solubility of inorganic reactants in solvents which can control the reaction level is another significant superiority. Here, we chose IPA as reaction medium to synthesize the 1D rod-like precursor $Na_7(H_3O)Nb_6O_{19}\cdot 14H_2O$, and 1D rod-like orthorhombic as well as ellipsoid-like monoclinic $NaNbO_3$ powders are successfully obtained by heat treatments. And possible mechanisms for temperature-induced phase transition and morphological evolution are further identified.

2. Experimental procedure

2.1. Synthesis and preparation

All chemicals were of analytical grade and used as received without further purification. In a typical solvothermal procedure for synthesizing the rod-like precursor $Na_7(H_3O)Nb_6O_{19}\cdot 14H_2O$, 2.083 g of sodium hydroxide (NaOH, 96% min,

Sinopharm Chemical Reagent Co., Ltd.) was dissolved into 50 mL of IPA (C_3H_8OH, 99.7% min, Sinopharm Chemical Reagent Co., Ltd.) through vigorous magnetic stirring. Niobium oxide (Nb_2O_5, 99.5%, Sinopharm Chemical Reagent Co., Ltd.) was added slowly into this solution after 30 min of stirring. The mixture was then stirred vigorously at room temperature for another 30 min, transferred to a Teflon-lined autoclave (70 mL), and heated to 230 ºC. After 16 h of heating, the mixture was naturally cooled to room temperature. The product was rinsed with de-ionized water and anhydrous alcohol, and precipitated with centrifugation for 5 min at 3000 rpm to yield a white, rod-like precursor powder. Rinsing was repeated thrice to remove excess ions from the final product, and the precursor was dried at 80 ºC overnight.

The as-obtained precursor was subjected to heat treatments in air at 300–800 ºC for 4 h to obtain the final products. The NaOH + IPA solution without Nb_2O_5 was stirred continuously both at room temperature and during heating, and a pH meter (EUTECH 510) recorded the pH of the mixture every 10 min to evaluate the solubility of NaOH in IPA solvent.

2.2. Characterization

The crystal structure of the as-prepared sample was characterized by a Bruker X-ray diffractometer (XRD, Bruker D8 Advance, Germany with a Cu Kα radiation (40 kV, 40 mA) source (λ = 0.154178 nm) at a scanning rate of 10^o/min in the 2θ range of 5º–60°. To analyze the thermal behavior of as-synthesized precursor, thermo-gravimetric analysis and differential scanning calorimetry (TGA-DSC, NETZSCH-STA 409PC, German) were conducted in Ar atmosphere at a heating rate

of 10°C/min from room temperature to 900 °C. Using a 514.5 nm laser, Raman spectra were measured by a confocal laser micro-Raman spectroscopy system (Raman, LABRAM HR800) within the range of 100 – 1000 cm^{-1}. The morphology and microstructure of as-synthesized samples were observed using a Hitachi S-4800 field emission scanning electron microscope (FE-SEM, Hitachi S-4800, Japan) and a transmission electron microscope (TEM; JEOL JEM-2100, Japan).

3. Results and discussion

3.1. Synthesis of $Na_7(H_3O)Nb_6O_{19}.14H_2O$

Figure 1 shows the crystalline structure of as-obtained product determined by XRD pattern. The sample is identified as orthorhombic-phase $Na_7(H_3O)Nb_6O_{19}.14H_2O$ (JCPDS Standard Card No.: 84-0188; Space group: *Pmnn*; Lattice parameters: a = 10.072 Å, b = 12.148 Å, c = 12.722 Å). This result reveals an important fact that $Na_7(H_3O)Nb_6O_{19}.14H_2O$ can be formed at a relatively low alkalinity of 1 M, owing to the unique characteristics of IPA, including polarity, viscosity, surface tension, and boiling point, *etc*.[35] Conventionally, synthesizing the same products *via* hydrothermal route requires a higher alkalinity ranging from 10 M to 15 M, and the formation process is difficult to control.[36-38] The IPA-based solvothermal strategy provides a facile, controllable, and moderate process for obtaining intermediate $Na_7(H_3O)Nb_6O_{19}.14H_2O$ and can be extended to the selective synthesis of the other multiphase materials.

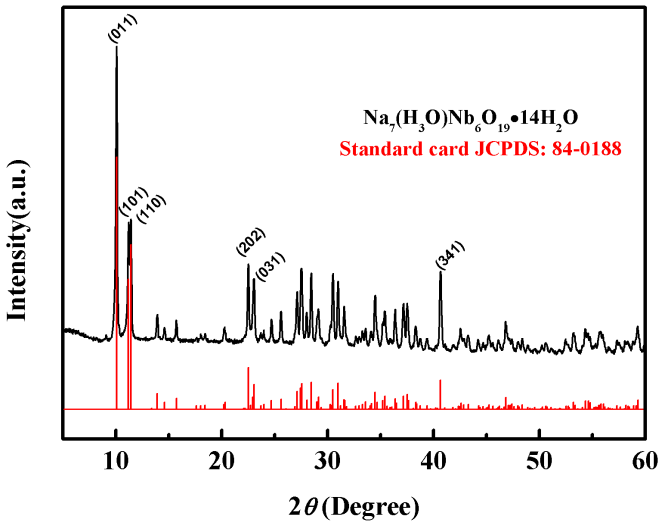

Figure 1. Powder XRD patterns of as-synthesized precursor using organic solvent isopropanol as reaction medium (230ºC, 16h).

In a previous study, alkaline niobate powders were synthesized in solution *via* a dissolution-precipitation process,[39] and the pertinent reaction processes can be written as follows:[40]

$$Nb_2O_5+8OH^-\rightarrow Nb_6O_{19}^{8-}+H_2O \quad (1)$$

$$Nb_6O_{19}^{8-}+34OH^-\rightarrow NbO_6^{7-}+17H_2O \quad (2)$$

$$A^+ + NbO_6^{7-}+3H_2O\rightarrow ANbO_3+6OH^- \quad (3)$$

A^+ in reaction (3) refers to alkali ions, such as Na^+ and K^+. Reactions (1) and (2) show that the alkaline concentration required for the formation of NbO_6^{7-} anions from $Nb_6O_{19}^{8-}$ should be higher than that necessary for the dissolution of Nb_2O_5. Actually, the pH value of the designed 1 M NaOH+IPA solution reaches 13.2 through vigorous stirring and heating (Figure 2). The pH value range is beneficial for the stable existence of $Nb_6O_{19}^{8-}$.[41] Therefore, the actual OH^- concentration is limited, and the

reaction process can only proceed to step (1), while step (2) requiring higher alkaline concentration would not occur. This may be a necessary factor accountable for the stable synthesis of $Na_7(H_3O)Nb_6O_{19}\cdot 14H_2O$ in organic solvent IPA. However, almost all the previous reported solvothermal synthesis of alkali niobates are conducted in mixture solutions of water and organic solvents, and the unique effects of organic solvents cannot work out effectively. [27-29] Thus, solvothermal route using pure organic solvent as reaction medium is considered to be a promising method in synthesizing niobate and other organic powders.

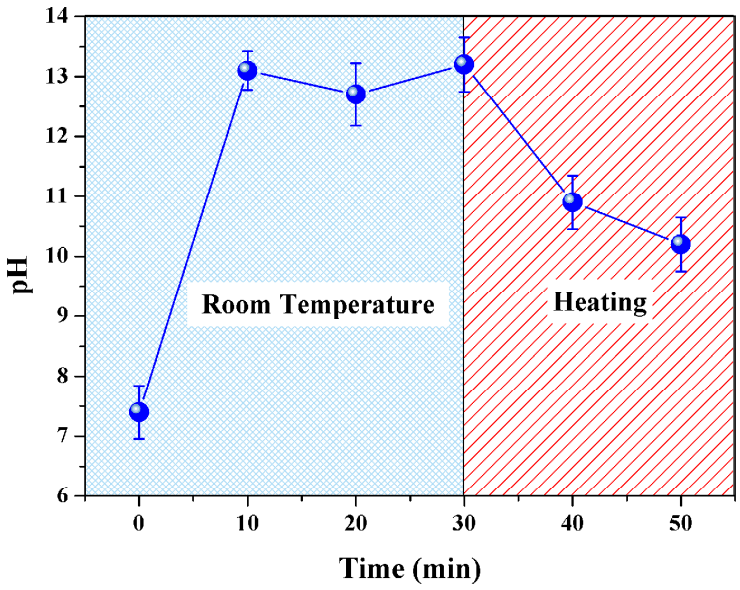

Figure 2. Solubility of NaOH in organic isopropanol solvent at room temperature and heating condition evaluated by the pH value as a function of time. Results are presented as mean ± SEM (error bar).

Figure 3 shows the DSC-TGA curves of the precursor heated from room temperature to 900 ºC. Significant weight loss is observed as the temperature increased from 80 ºC to 200 ºC, which is attributed to the elimination of crystallization water and hydration

water from $Na_7(H_3O)Nb_6O_{19}.14H_2O$. With further increases of temperature, the mass loss rate slows down and ceases at about 300 ºC. The weight loss observed is highly similar to that found in the thermogram of the same product prepared by the molten method, corresponding to the mass of 14.4 H_2O.[42] As the temperature increased from 600 ºC to 800 ºC, a slight weight loss of ~2% can be observed, which is attributed to the evaporation of sodium ions. The DSC plot for the decomposition of the product in Ar gas shows four peaks (blue curve in Figure 3). The first peak at 122 ºC indicates an endothermic event corresponding to the rapid release of H_2O. The second peak at 414 ºC presents the transformation of the precursors into the $NaNbO_3$ phase. The remaining peaks, which are located at 585 and 856 ºC, are likely related to the phase transition of $NaNbO_3$. This transition will be clarified in the phase structure analysis in the next section.

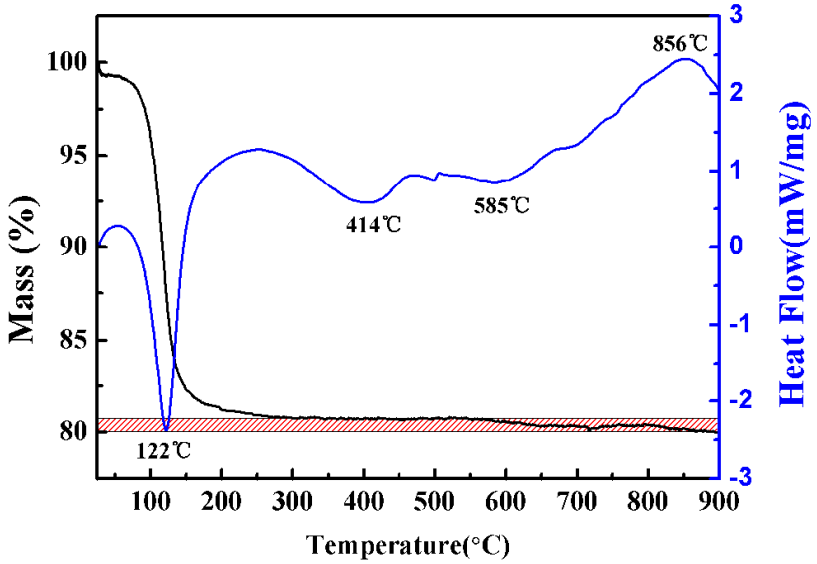

Figure 3. DSC-TG curves of as-synthesized $Na_7(H_3O)Nb_6O_{19}\cdot 14H_2O$.

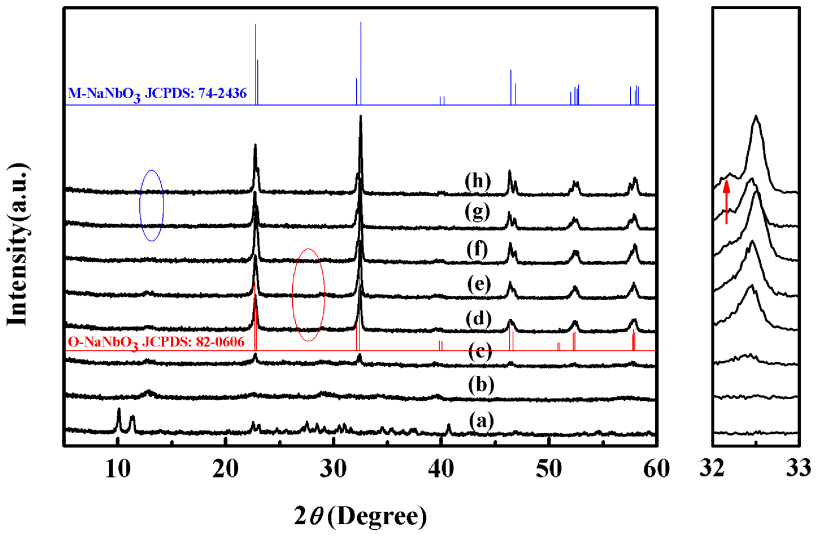

Figure 4. Powder XRD patterns of (a) $Na_7(H_3O)Nb_6O_{19}\cdot 14H_2O$ obtained solvothermally, and calcined in air at various temperature for 4h: (b)300ºC, (c)350ºC, (d)400ºC, (e)500ºC, (f)600ºC, (g)700ºC, (h)800ºC.

3.2. Phase structure analysis of the powder after annealing

Annealing treatments from 300 ºC to 800 ºC were conducted based on the DSC-TGA results. Figure 4 shows the XRD patterns of the powders obtained after annealing. Figure 4(a) displays the XRD pattern of as-prepared $Na_7(H_3O)Nb_6O_{19}\cdot 14H_2O$ for comparison. After heating treatment at 300 ºC for 4 h, the strong characteristic diffraction peaks [(011)/(101)/(110)] of $Na_7(H_3O)Nb_6O_{19}.14H_2O$ disappear, and no other diffraction peaks is observed [Figure 4(b)]. When the annealing temperature increased to 350 ºC, two diffraction peaks at 2θ of 22º and 32º are observed, as shown in Figure 4(c). As the temperature continuously increased to 400 ºC [Figure 4(d)], the intensity of the diffraction peaks is significantly enhanced and these peaks can be indexed to the orthorhombic perovskite structure of $NaNbO_3$ (JCPDS Standard Card

No.: 82-0606, Space group: *P*21ma, Lattice parameters: a = 5.569Å, b = 7.790 Å, c = 5.518 Å). During annealing at 400 °C, the transient $Na_7(H_3O)Nb_6O_{19}.14H_2O$ phase may be expected to transform into the orthorhombic $NaNbO_3$ (O-$NaNbO_3$). A similar transformation has been observed upon formation of $K_xNa_{1-x}NbO_3$ nanorods.[43] Figures 4(d)–4(f) demonstrate that when the temperature rises to 600 ºC, the O-$NaNbO_3$ is maintained and the intensity of the diffraction peaks is further increased. Moreover, the diffraction peaks shift slightly to a higher diffraction angle. The crystal parameters slightly decrease based on the Bragg equation ($2d\sin\theta=\lambda$). As the temperature increased from 600 ºC to 700 ºC, the diffraction peaks shift to a lower angle, which is attributed to the transformation of the phase structure of the products, as evidenced by appearance of a new peak [marked by a red arrow in the magnified Figure 4(g)]. This peak is attributed to monoclinic $NaNbO_3$ (M-$NaNbO_3$, JCPDS Standard Card No.: 74-2436; Space group: *P*2/m; Lattice parameters: a=3.909Å, b=3.871 Å, c=3.909Å, β=90.53°). Moreover, by increasing the temperature to 800 ºC, as shown in Figure 3(h), the diffraction peaks shift to the higher angles and their intensities are enhanced. The strong dependence of the phase transformations of niobium oxide on the heat treatments has also been evidenced by Raman spectra as shown in Fig S1.

Table 1. Crystal structure of the $Na_7(H_3O)Nb_6O_{19}\cdot 14H_2O$ synthesized solvothermally and the relative $NaNbO_3$ samples obtained at different thermal treatment temperature

Temperature (°C)	Material	Crystal system	Space group	Lattice parameters a(Å)	b(Å)	c(Å)	α(º)	β(º)	γ(º)
Precursor	$Na_7(H_3O)Nb_6O_{19}\cdot 14H_2O$	Orthorhombic	Pmnn(58)	10.074(2)	12.136(1)	12.7334	90	90	90
400	$NaNbO_3$	Orthorhombic	Pm21(26)	5.536(8)	7.814(4)	5.519(1)	90	90	90
500	$NaNbO_3$	Orthorhombic	Pm21(26)	5.518(7)	7.804(8)	5.498(1)	90	90	90
600	$NaNbO_3$	Orthorhombic	Pm21(26)	5.478(8)	7.793(6)	5.493(2)	90	90	90
700	$NaNbO_3$	Monoclinic	P2/m(10)	3.929(3)	3.879(2)	3.919(9)	90	90.6	90
800	$NaNbO_3$	Monoclinic	P2/m(10)	3.913(3)	3.870(3)	3.914(1)	90	90.57	90

Table 1 lists the lattice parameters of all of the samples. An increase in temperature gives rise to a gradual decrease among the lattice parameters of both orthorhombic and monoclinic $NaNbO_3$, which is in accordance with the shifting of peaks in the XRD patterns [Figures 4(d)–4(h)]. The evaporation of alkali metal elements A (A = Li, Na, K) at high temperatures can shift the diffraction peaks of alkali niobates to a higher angle (including $KNbO_3$, $NaNbO_3$, $LiNbO_3$, and their solid solutions).[44, 45] However, the temperature-dependent shift of the diffraction peaks below 600 ºC has never been reported. Thus, we propose a possible mechanism based on the formation process of $NaNbO_3$ to explain this shift.

In solvothermally synthesized $Na_7(H_3O)Nb_6O_{19}.14H_2O$, the position of Na may be partially occupied by H_3O^+ because the ionic radius of Na^+ (~1.54 Å) is similar to that of H_3O^+ (~1.35 Å).[46] Through dehydration and decomposition during heating

treatment, sodium vacancies are produced after the elimination of crystal water. These sodium vacancies are unstable, and the unit cell will shrink to decrease the volume of the vacancies through adequate driving forces from the external environment. An increase in temperature aggravates the level of shrinkage, as reflected by the shift of diffraction peaks to higher angles.

Compositional analysis was conducted by energy-dispersive X-ray spectroscopy (EDS), and Figure 5 shows the ratio of Na/Nb as a function of temperature. The ratio of Na/Nb at 400 and 600 ºC changed vanishingly (Δ1), which confirms that the shrinkage of lattice parameters is not mainly induced by the evaporation of alkali metal elements. As the temperature increased from 600 ºC to 800 ºC, the ratio of Na/Nb decreases sharply (Δ2, 13.44 times of Δ1), disclosing that the evident decrease in Na resulted from evaporation at such temperatures shifts the diffraction of M-$NaNbO_3$ to higher angles [Figure 4(h)] and changes O-$NaNbO_3$ [Figure 4(f)] to M-$NaNbO_3$ [Figure 4(g)]. From XRD (Fig 4) and EDS (Fig S2) results, we can conclude that the present systems are of high purity. Temperature-medaited crystal structure transformation is a complex process involving dehydration, decomposition, and element volatilization. Understanding this reaction mechanism is essential to prepare varying crystals of the desirable phases.

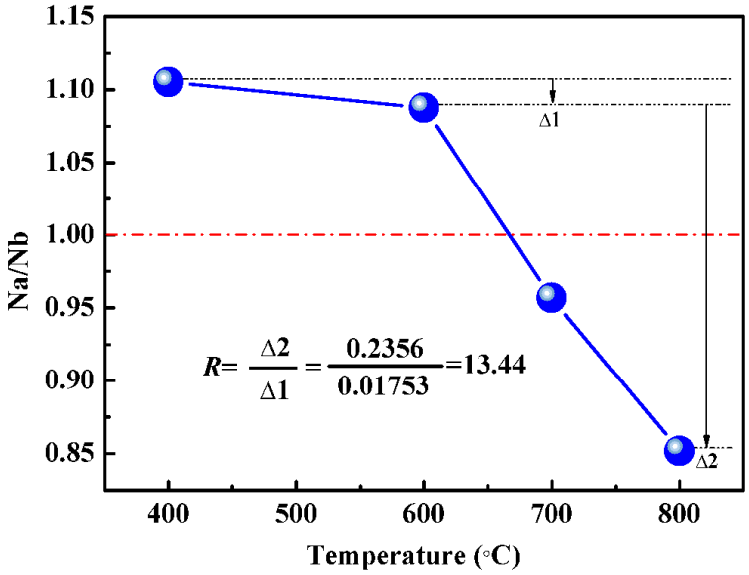

Figure 5. The molar ratio value of Na/Nb of the samples obtained at different calcination temperatures.

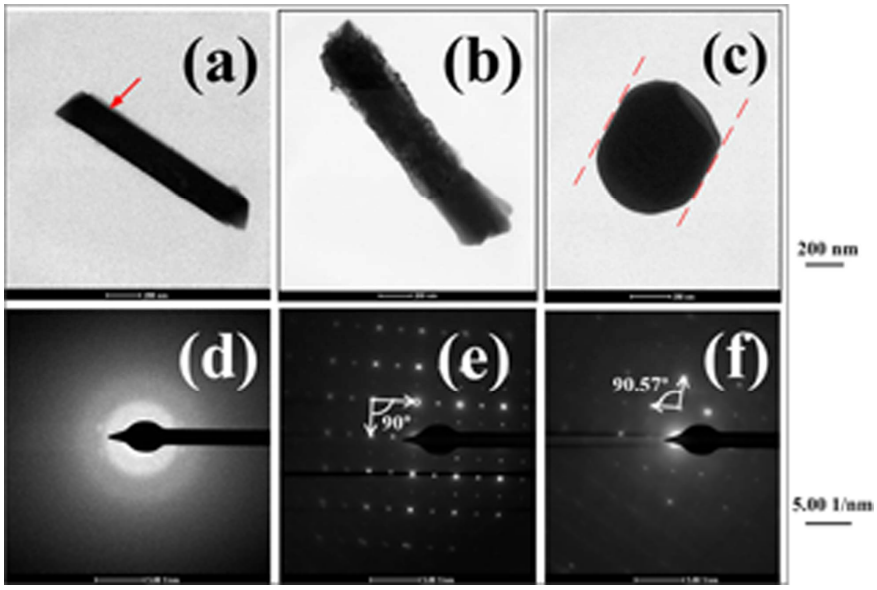

Figure 6. (a, b, c) Transmission electron microscope (TEM) images and (d, e, f) corresponding selective area electron diffraction (SAED) pattern of (a, d) $Na_7(H_3O)Nb_6O_{19}.14H_2O$; (b, e) Orthorhombic $NaNbO_3$; (c, f) monoclinic $NaNbO_3$.

3.3. Morphology evolutions of the powders after annealing

The morphology, grain size, and crystal structure of the samples are investigated by TEM and SAED (Figure 6). As observed, individual $Na_7(H_3O)Nb_6O_{19}\cdot 14H_2O$ has a rod-like shape with a width and length of 193.2 ± 1.3 and 1193.8 ±53.1 nm, respectively. Compared with that described in previous reports, this precursor displays a square-shaped cross section [marked by a red arrow in Figure 6(a)], and the surfaces of the rod are smoother and more compact. It should be pointed out that $Na_7(H_3O)Nb_6O_{19}\cdot 14H_2O$ is not particularly stable, as it prefers being decomposed and transformed into poor crystallites or amorphous states upon heating treatment [Figure 4(b)]. Such decomposition and transformation processes might happen by irradiation of a high-energy electron beam during TEM characterization. Therefore, it is reasonable that the SAED patterns of $Na_7(H_3O)Nb_6O_{19}\cdot 14H_2O$ shows an amorphous facula [Figure 6(d)]. As shown in Figure 6(b), O-$NaNbO_3$ also possesses the rod-like shape. Though its morphology is similar to the $Na_7(H_3O)Nb_6O_{19}\cdot 14H_2O$, the microstructure of O-$NaNbO_3$ becomes looser, more rough, and more irregular, with the increased width and length of 305.1 ± 15.5 and 1505.6 ± 90.0 nm, respectively. As for M-$NaNbO_3$, its morphologies drastically changed from the original rods into near-ellipsoid shapes of 512.3 ± 16.2 nm in width and 548.6 ± 42.9 nm length [Figure 6(c)]. The two opposite edges of the ellipsoid appear to be parallel to each other whereas the other two present apparent radians, which should be related to the square-shaped rod-like nature of the $Na_7(H_3O)Nb_6O_{19}\cdot 14H_2O$ precursor. As revealed by the SAED patterns in Figures 6(e) and 6(f), both M-$NaNbO_3$ and O-$NaNbO_3$

present fine crystallites. Additionally, a more detailed statistical analysis reporting the size distribution of the powders is shown in Fig S3. The size distribution results are obtained from several TEM images, and Figs S3(a), (d) and (g) are the representative TEM image of samples prepared solvothermally and treated at 400°C and 600°C, respectively. After the heat treatment at 400°C [Figs S3 (e) and (f)], the average size of powders slightly increases both in length and width compared to the solvothermal prepared samples [Figs S3 (b) and (c)].

Apparent differences in the microstructure, shape, and grain size of each phase motivated deep studies on the morphological evolution of the products. Figure 8 shows the FE-SEM images of the products obtained as a function of the annealing temperature. The images obtained highlight the importance of temperature on the morphological evolution of the products. Figure 7(b), for example, shows that the main shape and size of the sample obtained after heating at 300 °C for 4 h are not significantly different from those of the $Na_7(H_3O)Nb_6O_{19}\cdot 14H_2O$ precursors [Figure 7(a)]. However, a small amount of white particles appeared on the surface of the rods. As the temperature increased to 350 °C [Figure 7(c)] and 400 °C [Figure 7(d)], the basic rod structures become loosened and grainy, while white particles on the surfaces of the structures disappears. As previously reported,[42] the transition from $Na_7(H_3O)Nb_6O_{19}\cdot 14H_2O$ to $NaNbO_3$ would generate a certain amount of NaOH (Melting point: 318°C). Hence, the white particles here are inferred to be NaOH, and the disappearance at 350°C is resulted from their molten.

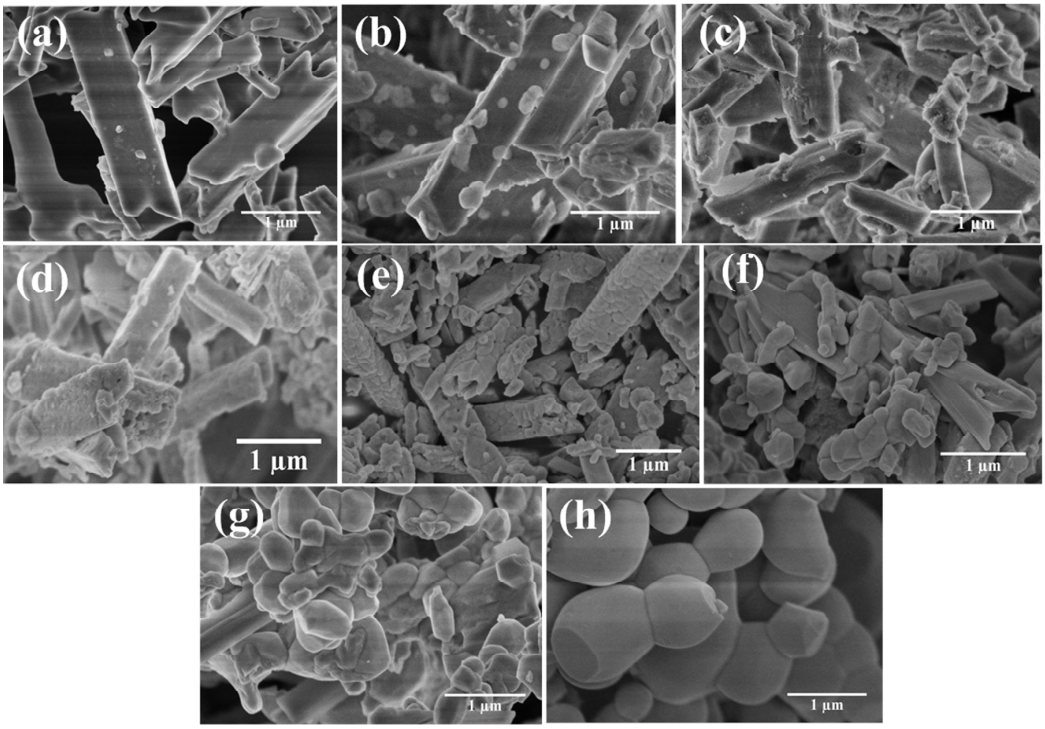

Figure 7. Temperature-induced morphology evolution observed by FE-SEM: (a)as-synthesized $Na_7(H_3O)Nb_6O_{19}\cdot 14H_2O$; (b)300ºC, (c)350ºC, (d)400 ºC, (e)500 ºC, (f)600 ºC, (g)700 ºC, (h)800 ºC.

When the annealing temperature is increased to 500 and 600 °C [Figures 7(e) and (f)], the rod-like shapes are still maintained as the grains grow into the average sizes of 180 and 400 nm, respectively, at the expense of small grains. It is notable that some cavities are generated in the rods, and higher temperatures slightly collapse the rod-like shapes to form dispersive particles [Figure 7(f)]. Therefore, the binding force between the particles is decreased as the temperature increasing. Nano-scalar particles can be obtained through ultrasonic treatment of the loose rods; such treatment provides a novel method for preparation of nanoparticles (NPs) from destruction of micro-rods (MRs). The size of the NPs may be controlled by tailoring the aspect ratio of the MRs. The work on this topic is currently underway.

Figures 7(g) and 7(h) show FE-SEM images of the samples obtained after thermal treatments above 700 °C. No trace of the rod-like structure is observed in these images, and all of the particles appear as irregular ellipsoids. By increasing the temperature from 700 °C to 800 °C, the ellipsoid-like grains grow rapidly from ~500 nm to ~1 μm with a broad size distribution.

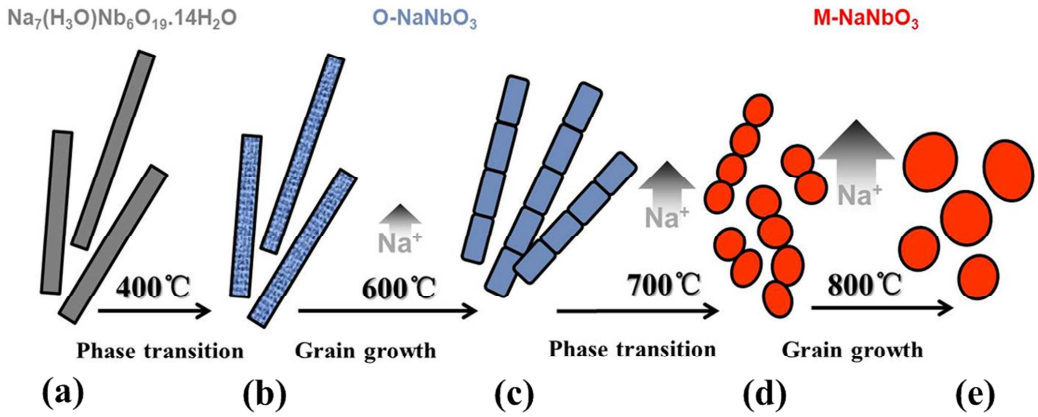

Figure 8. Schematic illustration of phase transitions and morphology evolutions induced by various calcination temperatures.

3.4. Mechanisms of morphological evolution

Figure 8 schematically illustrates the crystal structure and morphology transformation during subsequent calcination of $Na_7(H_3O)Nb_6O_{19}\cdot14H_2O$. When the temperature is increased to 400 °C, as-synthesized $Na_7(H_3O)Nb_6O_{19}\cdot14H_2O$ is converted into the orthorhombic-structured $NaNbO_3$ without changing its basic rod-like shape. Given that the transformation process involves (a) the dehydration reaction from $Na_7(H_3O)Nb_6O_{19}\cdot14H_2O$ to $Na_7[HNb_6O_{19}]$ and (b) the decomposition reaction from $Na_7[HNb_6O_{19}]$ to O-$NaNbO_3$ and NaOH, the structure of the rod-like O-$NaNbO_3$ becomes looser as it is composed of a large amount of tiny grains with high surface energy. Similar rough interconnected crystalline structures have been observed in

solvothermal synthesized metal oxides (including TiO_2, SnO_2, In_2O_3 and PbO).[47] The changes in structure and morphology are considered to be originated from the phase transformation (for example, from anatase to rutile in TiO_2) as well as the growth of crystallites at higher annealing temperatures. However, XRD and SEM results indicate that, the morphology in our work can be derived from the initial formation of $NaNbO_3$ from decomposition process and the growth of crystallites. As temperature increased to 700°C, phase transformation from orthorhombic to monoclinic occurs, and the crystallites growth process continues. The results indicate that the phase transformation from orthorhombic to monoclinic is oriented rearrangement process, and cannot bring evident changes in morphology. Likewise, the rod/wire-like O-$NaNbO_3$ obtained from the intermediate phase $Na_2Nb_2O_6{\cdot}nH_2O$ has a surface that is as smooth as that of $Na_2Nb_2O_6{\cdot}nH_2O$.[18-24] The evaporation of alkali ions at high temperature is inevitable, especially at temperatures above 600 °C (Figure 4); this evaporation accounts for the phase transformation from O-$NaNbO_3$ to M-$NaNbO_3$.

4. Conclusions

A facile and stable solvothermal process is developed for synthesis of rod-like $Na_7(H_3O)Nb_6O_{19}{\cdot}14H_2O$, and IPA is found to be a favorable reaction medium. The $Na_7(H_3O)Nb_6O_{19}{\cdot}14H_2O$ precursor could be further transformed to $NaNbO_3$ with various crystal structures, shapes, and grain sizes by simple thermal treatments. Gradual increase of the heating temperature gives rise to transformation from rod-like $Na_7(H_3O)Nb_6O_{19}{\cdot}14H_2O$ to rod-like $Na_7[HNb_6O_{19}]$, rod-like O-$NaNbO_3$, and finally approximately ellipsoid-like M-$NaNbO_3$. The elimination H_3O^+ derived from

solvothermal synthesized precursors gives rise to the cell unites shrinkage at low temperature. Sodium ion evaporation accounts for the phase transformation from O-$NaNbO_3$ to M-$NaNbO_3$, while decomposition from $Na_7(H_3O)Nb_6O_{19}\cdot 14H_2O$ to $NaNbO_3$ and NaOH leads to the formation of loose, rod-like structures and eventual collapse of these rods into ellipsoid particles. This investigation on solvothermal synthesis, thermal-induced structures, and morphological transformations has been offering the foundation for property study and functional application of alkali niobates with desirable phase structures, morphologies, and sizes.

Acknowledgements

This work was supported by the National Nature Science Foundation of China (NSFC No. 51172108), A Project Funded by the Priority Academic Program Development of Jiangsu Higher Education Institutions

References

(1) W. Zeng, X. M. Tao, S. Chen, S. M. Shang, H. L. W. Chan, S. H. Choy, *Energy Environ. Sci.,* 2013, 6, 2631-2638.

(2) M. Blomqvist, S. Khartsev, A. Grishin, A.P etraru, C. Buchal, *Appl. Phys. Lett.,* 2003, 82, 439.

(3) F. Dutto, C. Raillon, K. Schenk, A. Radenovic, *Nano Lett.,* 2011, 11 (6), 2517–2521.

(4) C. L. Yan, L. Nikolova, A. Dadvand, C. Harnagea, A. Sarkissian, D. F. Perepichka, D. F. Xue, F. Rosei, *Adv. Mater*., 2010, 22(15), 1741–1745.

(5) J. H. Jung, M. Lee, J. I. Hong, Y. Ding, C. Y. Chen, L. J. Chou, Z. L. Wang, *ACS Nano,* 2011, 5(12), 10041–10046.

(6) Y. Saito, H. Takao, T. Tani, T. Nonoyama, K. Takatori, T. Homma, T. Nagaya, M. Nakamura, *Nature,* 2004, 432, 84–87.

(7) S. T. Lau, C. H. Cheng, S. H. Choy, D. M. Lin, K. W. Kwok, H. L. W. Chan, *J. Appl. Phys.,* 2008, 103, 104105.

(8) S. F. Chen, L. Ji, W. M. Tang, X. L. Fu, *Dalton Trans*., 2013, 42, 10759–10768.

(9) S. K. Mishra, N. Choudhury, S. L. Chaplot, P. S. R. Krishna, R. Mittal, *Phys. Rev. B*, 2007, 76, 024110.

(10) P. Li, S. X. Ouyang, Y. J. Zhang, T. Kako, J. H. Ye, *J. Mater. Chem. A,* 2013, 1, 1185–1191.

(11) T. T. Zhang, K. Zhao, J. G. Yu, J. Jin, Y. Qi, H. Q. Li, X. J. Hou, G. Liu, *Nanoscale,* 2013, 5, 8375–8383.

(12) D. R. Modeshia, R. J. Darton, S. E. Ashbrook, R. I. Walton, *Chem. Commun.,*

2009, 68–70.

(13) K. E. Johnston, C. C. Tang, J. E. Parker, K. S. Knight, P. Lightfoot, S. E. Ashbrook, *J. Am. Chem. Soc.,* 2010, 132(25), 8732–8746.

(14) K. J. Zhu, Y. Cao, X. H. Wang, L. Bai, J. H. Qiu, H. L. Ji, *CrystEngComm* 2012, 14, 411–416.

(15) J. Lv, T. Kako, Z. S. Li, Z. G. Zou, J. H. Ye, *J. Phys. Chem. C,* 2010, 114, 6157–6162.

(16) T. Y. Ke, H. A. Chen, H. S. Sheu, J. W. Yeh, H. N. Lin, C. Y. Lee, H. T. Chiu, *J. Phys. Chem. C,* 2008, 112, 8827–8831.

(17) C. Y. Xu, L. Zhen, R. Yang, Z. L. Wang, *J. Am. Chem. Soc.,* 2007, 129, 15444–15445.

(18) H. F. Shi, T. Z. Wang, J. Chen, C. Zhu, J. H. Ye, Z. G. Zou, *Catal Lett.,* 2011, 141, 525–530.

(19) H. W. Xu, M. Nyman, T. M. Nenoff, A. Navrotsky, *Chem. Mater.,* 2004, 16, 2034–2040.

(20) J. H. Jung, C. Y. Chen, W. W. Wu, J. I. Hong, B. K. Yun, Y. S. Zhou, N. Lee, W. Jo, L. J. Chen, L. J. Chou, Z. L. Wang, *J. Phys. Chem. C,* 2012, 116 (42), 22261–22265.

(21) A. Yu, J. S. Qian, L. Liu, H. Pan, X. F. Zhou, *Appl. Surf. Sci.,* 2012, 258, 3490–3496.

(22) H. F. Shi, X. K. Li, D. F. Wang, Y, P. Yuan, Z. G. Zou, J. H. Ye, *Catal Lett.,* 2009, 132, 205–212.

(23) A. J. Paula, M. A. Zaghete, E. Longo, J. A. Varela, *Eur. J. Inorg. Chem.,* 2008, 1300–1308.

(24) L. Liu, B. Li, D. H. Yu, Y. M. Cui, X. F. Zhou, W. P. Ding, *Chem. Commun.,* 2010, 46, 427–429.

(25) M. Zhang, M. Guo, Y. Zhou, *Int. J. Appl. Ceram. Technol.,* 2011, 8(3), 591–596.

(26) A. D. Handokoa, G. K. L. Goh, *Green Chem.,* 2010, 12, 680–687.

(27) H. H. Gu, K. J. Zhu, X. M. Pang, B. Shao, J. H. Qiu, H. L. Ji, *Ceram. Int.,* 2012, 38, 1807–1813.

(28) L. Bai, K. J. Zhu, L. K. Su, J. H. Qiu, H. L. Ji, *Mater. Lett.,* 2010, 64, 77–79.

(29) L. K. Su, K. J. Zhu, L. Bai, J. H. Qiu, H. L. Ji, *J Alloy Compd*., 2010, 493, 186–191.

(30) D. Koziej, C. Floryan, R. A. Sperling, A. J. Ehrlicher, D. Issadore, R. Westervelt, D. A. Weitz, *Nanoscale,* 2013, 5, 5468–5475.

(31) G. Xu, Z. H. Tao, Y. G. Zhao, Y. F. Zhang, Z. H. Ren, G. Shen, G. R. Han, X. Wei, *CrystEngComm*, 2013, 15, 1439-1444.

(32) H. Zhu, C. Hou, Y. J. Li, G. H. Zhao, X. Liu, K Hou, Y. F. Li, *Chem. Asian J.* 2013, 8(7), 1447-1454.

(33) H. H. Gu, K. J. Zhu, J. H. Qiu, H. L. Ji, Y. Cao, J. M. Jin, *J. Nanosci. Nanotechnol.* 2013, 13(2), 1317-1322.

(34) A. R. Katrizky, D. A. Nichols, M. Siskin, *Chem. Rev.* 2001, 101, 837-892.

(35) F. Chen, Y. J. Zhu, X. Y. Zhao, B. Q. Lu, J. Wu, *CrystEngComm,* 2013, 15, 4527–4531.

(36) H. W. Song, W. H. Ma, *Ceram. Int.,* 2011, 37, 877–882.

(37) T. M. Alam, M. Nyman, B. R. Cherry, J. M. Segall, L. E. Lybarger, *J. Am. Chem. Soc.,* 2004, 126 (17), 5610–5620.

(38) M. Tanaka, S. Fujihara, *Eur. J. Inorg. Chem.,* 2012, 1180–1185.

(39) H. Liu, C. G. Hu, Z. L. Wang, *Nano Lett.*, 2006, 6 (7), 1535–1540.

(40) Y. M. Hu, H. S. Gu, Z. L. Hu, W. N. Di, Y. Yuan, J. You, W. Q. Cao, Y.Wang, H. L. W. Chan, *Cryst. Growth Des.,* 2008, 8(3), 832–837.

(41) A. Goiffon, R. Granger, C. Bockel, B. Spinner, *Rev. Chim. Miner.*, 1973, 10(3), 487–502.

(42) S. Yamazoe, T. Kawawaki, T. Imai, T. Wada, *J. Ceram. Soc. Jpn*., 2010, 118(8), 741–744.

(43) H. B. Xu, M. R. Joung, J. S. Kim, S. Nahm, M. G. Kang, C.Y. Kang, S. J. Yoon, *Chem. Eng. J.,* 2012, 211–212, 16–21.

(44) W. F. Liang, D. Q. Xiao, W. J. Wu, X. H. Li, Y. Sun, J. G. Zhu, *Curr. Appl. Phys.,* 2011, 11, S138–S142.

(45) J. Fang, X. H. Wang, Z. B. Tian, C. F. Zhong, L. T. Li, *J. Am. Ceram. Soc.*, 2010, 93(11), 3552–3555.

(46) G. Cao, R. C. Haushalter, K. G. Strohmaier, *Inorg. Chem.,* 1993, 32 (2), 127–128.

(47) X. C. Jiang, Y. L. Wang, T. Herricks, Y. N. Xia, *J. Mater. Chem.,* 2004, 14, 6 95–703.